

MS-DETR: Multispectral Pedestrian Detection Transformer with Loosely Coupled Fusion and Modality-Balanced Optimization

Yinghui Xing, *Member, IEEE*, Song Wang, Shizhou Zhang, Guoqiang Liang, Xiuwei Zhang, and Yanning Zhang, *Senior Member, IEEE*

Abstract—Multispectral pedestrian detection is an important task for many around-the-clock applications, since the visible and thermal modalities can provide complementary information especially under low light conditions. Most of the available multispectral pedestrian detectors are based on non-end-to-end detectors, while in this paper, we propose MultiSpectral pedestrian DETection TRansformer (MS-DETR), an end-to-end multispectral pedestrian detector, which extends DETR into the field of multi-modal detection. MS-DETR consists of two modality-specific backbones and Transformer encoders, followed by a multi-modal Transformer decoder, and the visible and thermal features are fused in the multi-modal Transformer decoder. To well resist the misalignment between multi-modal images, we design a loosely coupled fusion strategy by sparsely sampling some keypoints from multi-modal features independently and fusing them with adaptively learned attention weights. Moreover, based on the insight that not only different modalities, but also different pedestrian instances tend to have different confidence scores to final detection, we further propose an instance-aware modality-balanced optimization strategy, which preserves visible and thermal decoder branches and aligns their predicted slots through an instance-wise dynamic loss. Our end-to-end MS-DETR shows superior performance on the challenging KAIST, CVC-14 and LLVIP benchmark datasets. The source code is available at <https://github.com/YinghuiXing/MS-DETR>.

Index Terms—Multispectral pedestrian detection, end-to-end detector, loosely coupled fusion, modality-balanced optimization

I. INTRODUCTION

PEDESTRIAN detection is a popular research topic in autonomous driving [1], automated video surveillance [2], and robotics. With the development of deep convolution neural networks (CNN), many works are proposed [3]–[13], which greatly boost the development of pedestrian detection. However, as visible cameras are sensitive to lighting conditions, even an excellent detector can not accurately detect the pedestrians in adverse environmental conditions [14], limiting many around-the-clock applications. To solve this problem, multispectral systems, which have two types of camera sensors, i.e. visible and thermal, have been introduced. Thermal infrared cameras capture infrared radiation emitted by objects. They are insensitive to illumination and weather changes, thus can provide complementary information under adverse illumination conditions.

Benefiting from the availability of KAIST dataset [15], some detection methods designed for visible modality are extended to multispectral cases [15]–[24]. With the development of

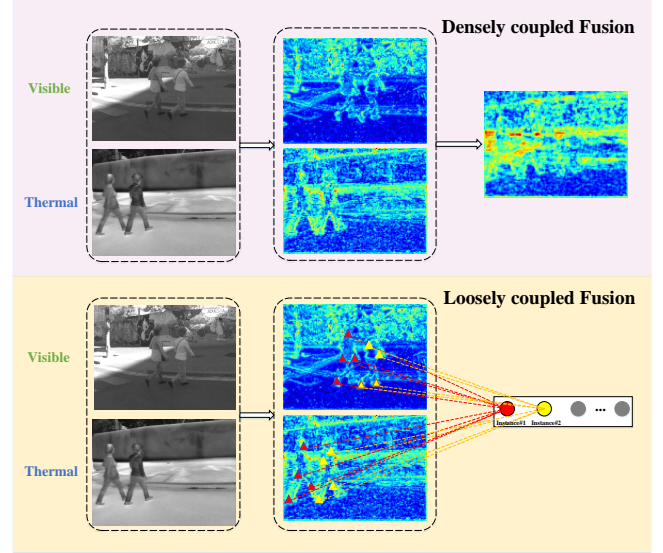


Fig. 1. Different fusion strategy of multispectral pedestrian detection. Densely coupled fusion, e.g., concatenation and addition, tends to drift from the target on the misaligned image pairs. In contrast, our loosely coupled fusion aggregates sampled keypoints, which is robust to resist the misalignment.

CNN on object detection, considerable progress has also been made on multispectral pedestrian detection. To the best of our knowledge, most of existing multispectral pedestrian detectors are all based on non-end-to-end detection models, which require some cumbersome modules, like pre-defined anchor boxes [25], a large scale of proposals [26] and non-maximum suppression (NMS).

Very recently, an end-to-end DETection TRansformer (DETR) [27] is proposed to reformulate object detection task as a direct set prediction problem. In this paper, we propose MultiSpectral pedestrian DETection TRansformer (MS-DETR) to extend the end-to-end DETR framework into the field of multispectral pedestrian detection. Our MS-DETR mainly contains two modality-specific CNN backbones and Transformer encoders, followed with a multi-modal Transformer decoder. Firstly, a ResNet-50 network combined with a Transformer encoder is adopted as the modality-specific feature extractor for the visible and thermal modality respectively. As for the multi-modal decoder, conventional densely coupled fusion strategies such as concatenation and addition would require strictly aligned features between the modalities when embed-

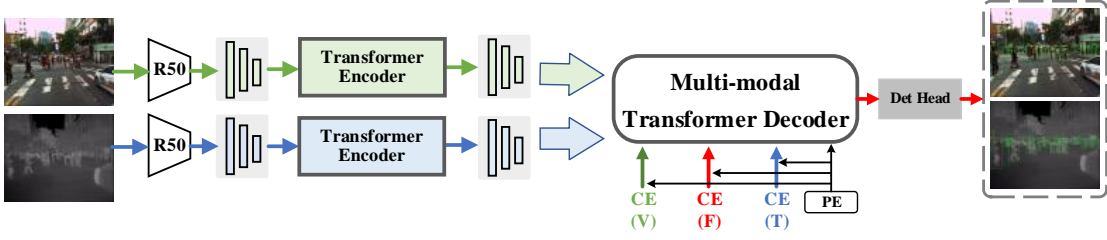


Fig. 2. Overall architecture of our MS-DETR, where two modality-specific CNN backbones and two modality-specific Transformer encoders are used for visible and thermal images feature extraction. The multi-modal Transformer decoder takes feature maps, positional encodings (PE) and modality-specific content embeddings (CE) as inputs to generate three sets of prediction slots. V, F, T are acronyms for visible, fusion, and thermal.

ded into the Transformer layers. However, most of multispectral pedestrian detection datasets, like KAIST and CVC-14, have some misaligned pedestrian pairs between visible and thermal modalities. Using such densely coupled fusion strategies may not well aggregate the prominent features, leading to inferior performance, as shown in Fig. 1. Therefore, to well suit the multi-modal decoder of MS-DETR, we introduce a loosely coupled fusion strategy instead. By sparsely sampling some keypoints and their corresponding attention weights from the two modalities independently, the multi-modal features are aggregated adaptively, which naturally avoids the strict aligned requirement between visible and thermal modalities.

From the other hand, during the optimization process of MS-DETR, it may be prone to be dominated by one of the modalities and the detector might suffer from the modality-imbalance problem [28], [29]. Generally speaking, in daytime, pedestrians in visible images include clearer texture features and in nighttime thermal images contain more distinct shape informations. While in many cases, pedestrians in thermal images still provide more obvious features than visible images in daytime such as the pedestrians stand in the shadow region or get over-exposed and vice versa. In other words, not only different modalities tend to obtain different confidence scores, but also each different pedestrian instance can have uneven contributions to the object losses under diverse illumination conditions. To alleviate this problem, we propose an instance-aware modality-balanced optimization strategy. To be specific, we additionally preserve visible and thermal decoder branches besides the fusion branch during the training phase. Based on the trident structure of the decoder, as shown in Fig. 3, we can then obtain three sets of predicted slots. Finally, an instance-wise dynamic loss is devised to adaptively adjust the contributions of each pedestrian instance to the model learning.

The main contributions of the paper are summarized as follows:

- We propose an end-to-end multispectral pedestrian detection model, dubbed as MS-DETR, which extends DETR from single-modal detection task into multispectral case by introducing a multi-modal Transformer decoder.
- A novel loosely coupled fusion strategy is proposed to improve the feature fusion efficiency towards multi-modal detection task. It shows great potential in DETR-like multi-modal framework compared with other fusion strategies.
- An instance-aware modality-balanced optimization strat-

egy is designed to align three sets of slots produced by three detection branches, i.e., visible, thermal and fusion branches. Based on these aligned slots, we use a dynamic loss to measure and adjust the contribution of each instance.

- We conduct thorough experiments to verify the effectiveness of the proposed method on three widely used datasets, namely KAIST, CVC-14, and LLVIP. Experimental results demonstrate the superiority of the proposed MS-DETR.

II. RELATED WORKS

A. Multispectral Pedestrian Detection

Since the release of large-scale multi-modal datasets like KAIST Multispectral Pedestrian Benchmark [15], CVC14 datasets [30], and LLVIP [31] etc, a variety of multispectral pedestrian detection methods were proposed [15]–[21], [23], [24], [32]–[38], [38]–[41]. Hwang *et al.* [15] extended the aggregated channel features (ACF) by incorporating the intensity and histogram of oriented gradient (HOG) features of the thermal channel to propose an ACF+T+THOG method. Choi *et al.* [16] argued that ACF+T+THOG features lacked discrimination in challenging circumstances, such as tiny appearance and bad visibility, then proposed to learn discriminative features through CNN and support vector regression (SVR). It is critical for multispectral pedestrian detectors to fuse multi-modal features. König *et al.* [17] developed a multispectral region proposal network (RPN) based on Faster R-CNN [25]. It fused the visible and thermal features by concatenation, and concluded that the best detection performance was obtained through halfway fusion [18].

Apart from concatenation, there are other fusion strategies. Park *et al.* [19] estimated the detection probabilities of different modalities by a channel weighting fusion layer, and then utilized an accumulated probability fusion layer to combine them. Some works incorporated illumination information of images as prior knowledge, and introduced illumination-aware networks to adaptively merge visible and thermal features [20], [21], [23]. Guan *et al.* [21] developed a two-stream deep neural networks, which not only utilized two illumination-aware networks to produce fusion weights, but also trained the detector by jointly learning pedestrian detection and semantic segmentation tasks. Actually, many works [21], [23], [32], [33] used semantic segmentation as an auxiliary task, which was proved to be an effective way to

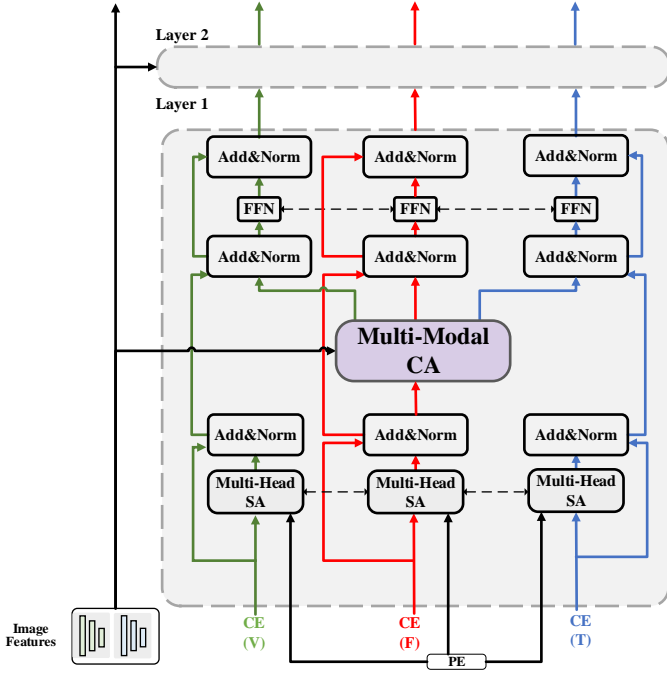


Fig. 3. The multi-modal Transformer decoder of MS-DETR. It has three branches, i.e. visible (V), fusion (F), and thermal (T), where PE, CE, SA, CA and FFN are acronyms for Positional Encodings, Content Embeddings, Self-Attention, Cross-Attention and feed forward network. Dashed lines indicate shared parameters.

boost the performance of multispectral pedestrian detection. Except for methods who made use of illumination information, Kim *et al.* [24] approached an uncertainty-aware multispectral pedestrian detection framework, which considered two types of uncertainties and fused the multispectral features by an uncertainty-aware feature fusion module. Li *et al.* [34] used the dense fusion strategy to extract multilevel multispectral representations and then combined the prediction results of different modalities based on Dempster’s rule of combination. It not only integrated multi-modal information, but also provided a reliable prediction.

Recently, some researchers emphasized the misalignment problem of KAIST [15] and CVC14 [30], and proposed some strategies to reduce the influence of modality-misalignment [35]–[37]. Zhang *et al.* [35] directly designed a Region Feature Alignment (RFA) module to adaptively compensate misalignment of feature maps in two modalities. Zhou *et al.* [36] developed an illumination-aware feature alignment module to select complementary features according to illumination conditions, which obtained better detection results. Aiming at the unpaired multispectral pedestrian detection issue, Kim *et al.* [37] leveraged multi-label learning to extract the state-aware features.

All above mentioned deep-learning based methods are anchor-based models. In this paper, we propose an end-to-end multispectral pedestrian detection model without the need of any anchor mechanism or the illumination/uncertainty prior, and is also robust to the misalignment of modalities.

B. End-to-end Object Detection

DETR [27], as one of the breakthroughs in object detection, treats object detection as a direct set prediction task without any hand-crafted prior knowledge like anchor generation or NMS. It is trained in an end-to-end manner with a set-based loss function, which performs bipartite matching between the predicted and the groundtruth bounding box [42]. DETR greatly simplifies the pipeline of object detection, and guides the tendency of object detection. Nevertheless, it suffers from slow training convergence. Several works have been proposed to improve it [43]–[48]. Conditional DETR [43] presented a conditional cross-attention mechanism to accelerate DETR’s training, and it converged $6.7\times$ faster than original DETR. Deformable DETR [46] was proposed to make the attention modules only attend to a small set of key sampling points around a reference, which makes it easy to aggregate multi-scale features. DAB-DETR [48] directly used box coordinates as queries to improve the query-to-feature similarity and to eliminate slow training convergence issue in DETR. Dynamic DETR [45] developed an alternative solution to boost the training convergence of DETR by replacing the cross-attention module in DETR decoder with an ROI-based dynamic attention.

Apart from the single-modal detectors, there are also some multi-modal detectors build upon DETR family. Kamath *et al.* [49] proposed an modulated detection model, MDETR, for end-to-end multi-modal understanding, where the visual and text features extracted from a convolutional backbone and a language model were concatenated and passed to the DETR [27] model for detection. However, the flattening operation on the visual features would destroy the spatial structure of images. Therefore, Maaz *et al.* [50] took the late multi-modal fusion strategy into MDETR framework and also introduced the multi-scale spatial context deformable attention to boost the training. Both of them are presented for vision-language alignment-related task, which is different from multispectral pedestrian detection that the inputs are both images.

III. PROPOSED METHOD

A. Overview

Based on deformable DETR, we propose MS-DETR, an end-to-end multispectral pedestrian detection model. As shown in Fig. 2, the proposed model is composed of three parts: two modality-specific CNN backbones, two modality-specific Transformer encoders and a multi-modal Transformer decoder.

Given a pair of visible image \mathbf{I}^V and thermal image \mathbf{I}^T , each modality-specific CNN backbone first extracts multi-scale feature maps. Then, these feature maps are fed into corresponding modality-specific encoder to aggregate the modality-specific multi-scale features through deformable self-attention. These two steps can be formulated as

$$\{\mathbf{E}_l^m\}_{l=1}^L = \phi^m(\varphi^m(\mathbf{I}^m)), m \in \{V, T\}, \quad (1)$$

where $\varphi^m(\cdot)$ and $\phi^m(\cdot)$ denote the CNN backbone and Transformer encoder of modality m . $\{\mathbf{E}_l^m\}_{l=1}^L$ represents the refined multi-scale feature maps, and l is the index of scale.

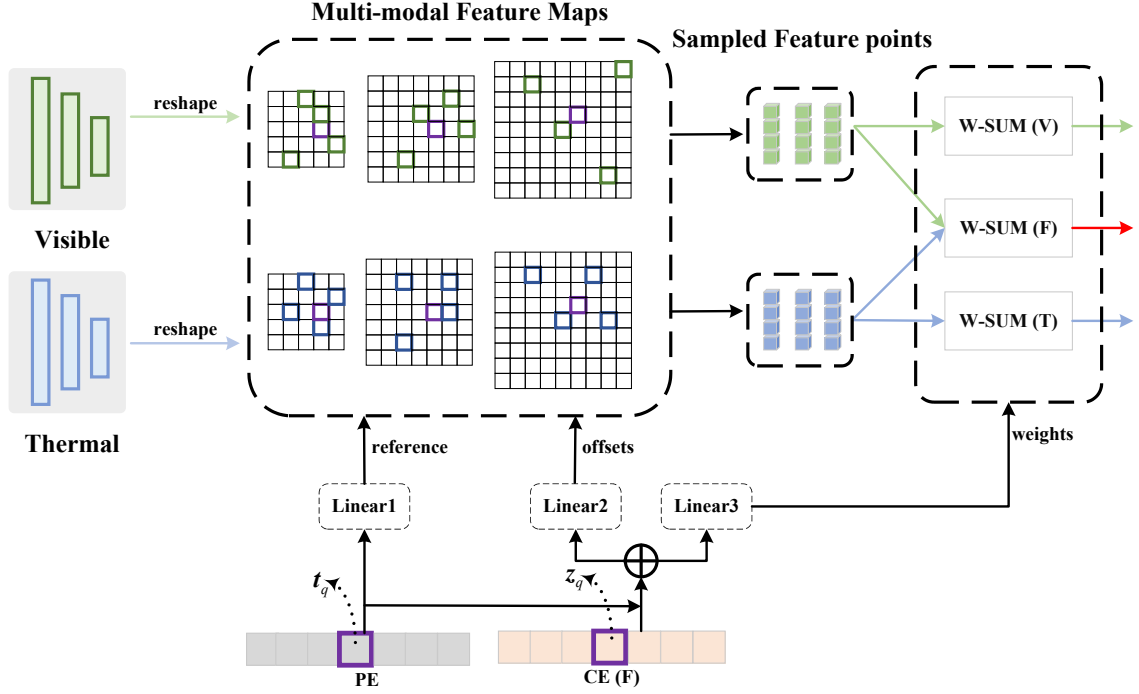


Fig. 4. Details of multi-modal cross-attention (CA) module. The positional encodings pass through a linear layer to predict reference points, and they are then combined with content embeddings of fusion branch to predict offsets and their corresponding attention weights. Given a group of reference points and offsets, two groups of feature points are sampled from multi-modal multi-scale features. These sampled feature points are fused by weighted sum operations.

The subsequent multi-modal Transformer decoder takes the multi-scale feature maps $\{\mathbf{E}_l^m\}_{l=1}^L$ of both modalities as the inputs. Besides, the learnable content embeddings (CE) combined with positional encodings (PE) are input to the decoder to perform cross-attention with the encoded input features. As shown in Fig. 3, instead of keeping the fusion branch alone, we preserve the visible and thermal branch additionally in the decoder. With the help of the constituted trident architecture, three sets of predicted slots can be obtained through the visible, thermal and fusion branches of the decoder, respectively.

To alleviate the modality-imbalance problem as stated previously, an instance-aware modality-balanced strategy is introduced to optimize the model. Specifically, an instance-wise dynamic weighting loss is enforced on top of the decoder to adaptively adjust the contributions of two modalities for each pedestrian instance.

Since our CNN backbones and modality-specific Transformer encoders are similar to previous works, we will not repeat them. Interested readers can refer to [46] for more details. In the following, we will elaborate the proposed multi-modal Transformer decoder and the instance-aware modality-balanced optimization strategy.

B. Multi-Modal Transformer Decoder

The detailed architecture of multi-modal Transformer decoder is shown in Fig. 3. In each layer, the multi-head Self-Attention (SA) and Feed-Forward Network (FFN) of visible (V), fusion (F) and thermal (T) branches have the same parameters, and all the three branches share a common multi-modal

cross-attention (CA) module. As the self-attention module and feed forward network in our multi-modal Transformer decoder is the same with that in DETR [27], we only focus on the novel multi-modal cross-attention module.

Multi-scale deformable attention in deformable DETR. Before elaborate the cross-attention module in our multi-modal Transformer decoder, we first briefly review that in deformable DETR [46].

For q -th object query, the 2D reference points $\hat{\mathbf{p}}_q$ are predicted from object queries via a learnable linear projection followed by a *sigmoid* function. Then the multi-scale deformable attention features are calculated by

$$\text{MSDeformAttn}(\mathbf{z}_q, \hat{\mathbf{p}}_q, \{\mathbf{E}_l\}_{l=1}^L) = \sum_{h=1}^H \mathbf{W}_h \left[\sum_{l=1}^L \sum_{k=1}^K A_{qhlk} \cdot \mathbf{W}'_h \mathbf{E}_l(\alpha_l(\hat{\mathbf{p}}_q) + \Delta \mathbf{p}_{qhlk}) \right], \quad (2)$$

where $\text{MSDeformAttn}(\cdot)$ denotes the multi-scale deformable attention in deformable DETR. \mathbf{z}_q is the content embedding of the q -th query. h , l , and k indicate the attention head, feature scale and sampling point, respectively. $\alpha_l(\hat{\mathbf{p}}_q)$ rescales $\hat{\mathbf{p}}_q$ to the input feature maps of the l -th scale. $\Delta \mathbf{p}_{qhlk}$ and A_{qhlk} represent the sampling offset and the scalar attention weight of the k -th sampling point in the l -th feature level for the h -th attention head. Note that in Deformable DETR, the sampling offsets and attention weights are obtained through linear layers.

Compared to the cross-attention in DETR, deformable cross-attention makes the model only focus on sparse and meaningful locations around a reference point, which greatly improves the computational and memory efficiency.

TABLE I
COMPARISONS WITH THE STATE-OF-THE-ART METHODS ON THE KAIST DATASET

Methods	MR^{-2} (IoU=0.5)					
	<i>Reasonable</i>			<i>All</i>		
	R-All	R-Day	R-Night	All	Day	Night
ACF [15]	47.32	42.57	56.17	67.74	64.32	75.06
Halfway Fusion [18]	25.75	24.88	26.59	49.20	47.67	52.35
Fusion RPN+BF [17]	18.29	19.57	16.27	51.67	52.30	51.09
IAF R-CNN [20]	15.73	14.55	18.26	44.24	42.47	47.70
IATDNN+IASS [21]	14.95	14.67	15.72	46.45	46.77	46.34
CIAN [38]	14.12	14.78	11.13	35.57	36.06	32.38
MSDS-RCNN [32]	11.34	10.54	12.94	34.20	32.12	38.83
AR-CNN [35]	9.34	9.94	8.38	34.95	34.36	36.12
DCRL(teacher) [23]	9.16	9.86	8.18	-	-	-
MBNet [36]	8.13	8.28	7.86	31.87	32.39	30.95
CMPD [34]	8.16	8.77	7.31	28.98	28.30	30.56
Kimet <i>al.</i> [24]	7.89	8.18	6.96	-	-	-
MLPD [37]	7.58	7.96	6.95	28.49	28.39	28.69
GAFF [22]	6.48	8.35	3.46	27.30	30.59	19.22
MS-DETR	6.13	7.78	3.18	20.64	22.76	15.77

"-" indicates the result is not provided.

Multi-modal cross-attention. Following the paradigm of deformable DETR, we extend it to a multi-modal case. Fig. 4 shows the detailed architecture of multi-modal cross-attention module. The positional encodings are firstly used to predict reference points. Specifically, the q -th positional encoding \mathbf{t}_q is taken into Linear1 to obtain the reference point's coordinates $\hat{\mathbf{p}}_q \in \mathbb{R}^2$,

$$\hat{\mathbf{p}}_q = \text{Linear1}(\mathbf{t}_q). \quad (3)$$

Meanwhile, the q -th positional encoding \mathbf{t}_q is also combined with content embedding of fusion branch \mathbf{z}_q to directly predict offsets of sampling points $\Delta \mathbf{p}_q \in \mathbb{R}^{|M| \times H \times L \times K \times 2}$ and their corresponding attention weights $\mathbf{a}_q \in \mathbb{R}^{|M| \times H \times L \times K}$ through two independent linear layers,

$$\begin{aligned} \Delta \mathbf{p}_q &= \text{Linear2}(\mathbf{z}_q + \mathbf{t}_q), \\ \mathbf{a}_q &= \text{Linear3}(\mathbf{z}_q + \mathbf{t}_q), \end{aligned} \quad (4)$$

where $M = \{V, T\}$ indicates the visible and thermal modalities, and $|M|$ is the number of modalities. H , L and K are the number of attention heads, features scales and the sampling points in a certain feature map.

After obtaining the prominent key elements and their corresponding attention weights of different feature scales and modalities, we use the softmax function to normalize these weights, i.e., $\mathbf{A}_q = \text{Softmax}(\mathbf{a}_q)$. Then the fused features can be obtained by

$$\text{Multi-ModalCA}_F = \sum_{h=1}^H \mathbf{W}_h \left[\sum_m \sum_{l=1}^L \sum_{k=1}^K A_{qmhkl} \cdot \mathbf{W}'_h \mathbf{E}_l^m (\alpha_l (\hat{\mathbf{p}}_q) + \Delta \mathbf{p}_{qmhkl}) \right] \quad (5)$$

We can observe from (5) that the fusion of visible and thermal features is only conducted during the process of aggregating prominent key elements of two modalities, thus we call it "loosely coupled fusion".

Based on the "loosely coupled fusion", we can easily introduce extra two detection branches to avoid under-optimizing uni-modal representation [28], [29]. As shown in Fig. 4, we

divide the offsets $\Delta \mathbf{p}_q$ into $\Delta \mathbf{p}_q^V$ and $\Delta \mathbf{p}_q^T$. Correspondingly, the attention weights \mathbf{a}_q are also splitted to two modality specific components \mathbf{a}_q^V and \mathbf{a}_q^T . After the normalization of softmax, we obtain the modality specific attention weights $\mathbf{A}_q^V = \text{Softmax}(\mathbf{a}_q^V)$ and $\mathbf{A}_q^T = \text{Softmax}(\mathbf{a}_q^T)$. Therefore, extra two groups of uni-modal features in the multi-modal cross-attention module are formulated by

$$\text{Multi-ModalCA}_V = \sum_{h=1}^H \mathbf{W}_h \left[\sum_{l=1}^L \sum_{k=1}^K A_{qhlk}^V \cdot \mathbf{W}'_h \mathbf{E}_l^V (\alpha_l (\hat{\mathbf{p}}_q) + \Delta \mathbf{p}_{qhlk}^V) \right], \quad (6)$$

$$\text{Multi-ModalCA}_T = \sum_{h=1}^H \mathbf{W}_h \left[\sum_{l=1}^L \sum_{k=1}^K A_{qhlk}^T \cdot \mathbf{W}'_h \mathbf{E}_l^T (\alpha_l (\hat{\mathbf{p}}_q) + \Delta \mathbf{p}_{qhlk}^T) \right]. \quad (7)$$

C. Instance-aware Modality-Balanced Optimization

By passing the decoder output to the modality-specific detection head, we can obtain three sets of predictions. Let $i \in \{V, T, F\}$ indicates different branches, these predictions can be represented by $\{\hat{y}_n^i\}_{n=1}^N$, $i \in \{V, T, F\}$. As the distinct characteristics of visible and thermal images, their predictions may not be consistent. To balance the contribution of different modalities, we compare and then select the optimal permutation of slots predictions in current iteration. After that, the predictions of all the three branches are re-arranged according to the selected permutation $\hat{\sigma}$.

To obtain $\hat{\sigma}$, we should firstly calculate the optimal permutation for each branch i

$$\hat{\sigma}^i = \arg \min_{\sigma \in \mathbb{S}_N} \sum_{n=1}^N \mathcal{L}_{\text{match}} \left(y_n, \hat{y}_{\sigma(n)}^i \right), i \in \{V, T, F\}, \quad (8)$$

where $\mathcal{L}_{\text{match}} \left(y_n, \hat{y}_{\sigma(n)}^i \right)$ is the matching cost between ground-truth y_n and the prediction produced by $\sigma(n)$ -th anchor

TABLE II
PERFORMANCE COMPARISONS ON THE SIX SUBSETS OF KAIST DATASET

Methods	Near	Medium	Far	None	Partial	Heavy	All
ACF [15]	28.74	53.67	88.20	62.94	81.40	88.08	67.74
Halfway Fusion [18]	8.13	30.34	75.70	43.13	65.21	74.36	49.20
Fusion RPN+BF [17]	0.04	30.87	88.86	47.45	56.10	72.20	51.67
IAF R-CNN [20]	0.96	25.54	77.84	40.17	48.40	69.76	44.24
IATDNN+IASS [21]	0.04	28.55	83.42	45.43	46.25	64.57	46.45
CIAN [38]	3.71	19.04	55.82	30.31	41.57	62.48	35.57
MSDS-RCNN [32]	1.29	16.18	63.76	29.94	38.46	63.30	34.20
DCRL(teacher) [23]	-	-	-	-	-	-	-
Kimet <i>al.</i> [24]	-	-	-	-	-	-	-
AR-CNN [35]	0.00	16.08	69.00	31.40	38.63	55.73	34.95
MBNet [36]	0.00	16.07	55.99	27.74	35.43	59.14	31.87
CMPD [34]	0.00	12.99	51.22	24.04	33.88	59.37	28.98
MLPD [37]	0.00	12.10	52.79	25.18	29.84	55.05	28.49
GAFF [22]	0.00	13.23	46.87	23.83	24.31	47.97	27.30
MS-DETR	0.00	9.70	32.41	16.54	23.61	48.71	20.64

"-" indicates the result is not provided.

box of modality i , and can be computed by

$$\begin{aligned} \mathcal{L}_{match} \left(y_n, \hat{y}_{\sigma(n)}^i \right) &= \mathcal{L}_{focal} \left(y_n, \hat{y}_{\sigma(n)}^i \right) + \mathcal{L}_{L1} \left(y_n, \hat{y}_{\sigma(n)}^i \right) \\ &\quad + \mathcal{L}_{GIoU} \left(y_n, \hat{y}_{\sigma(n)}^i \right). \end{aligned} \quad (9)$$

By comparing the matching costs under the permutations $\hat{\sigma}^V$, $\hat{\sigma}^T$ and $\hat{\sigma}^F$, we obtain the optimal permutation

$$\hat{\sigma} = \arg \min_{\sigma \in \{\hat{\sigma}^i\}} \sum_{n=1}^N \mathcal{L}_{match} \left(y_n, \hat{y}_{\sigma(n)}^i \right), i \in \{V, T, F\}. \quad (10)$$

Then, the slots of other branches are re-arranged according to $\hat{\sigma}$, and their matching costs are updated under the new permutation. In order to further boost the detection performance and to balance the training, we propose an instance-wise dynamic loss. Specifically, the matching costs are calculated under the optimal permutation in instance-level, and then, they are utilized to measure the degree of prediction confidence for different instances to adaptively adjust the instance-level weights of three branch. Suppose that there are T pedestrian instances, we use $c_{\hat{\sigma}(j)}^i$ to represent the instance-level matching cost of j -th instance in modality i under the optimal permutation $\hat{\sigma}$. The dynamic fusion parameters $\lambda_{\hat{\sigma}(j)}^i$, ($i \in \{V, T, F\}$) are obtained through

$$\lambda_{\hat{\sigma}(j)}^i = \frac{e^{c_{\hat{\sigma}(j)}^i}}{e^{c_{\hat{\sigma}(j)}^V} + e^{c_{\hat{\sigma}(j)}^F} + e^{c_{\hat{\sigma}(j)}^T}}, j = 1, \dots, T. \quad (11)$$

Then the loss of modality i is composed of a dynamic loss term for predicted pedestrians and a focal loss term for predicted non-pedestrians:

$$\mathcal{L}^i = \sum_{s=1}^T \lambda_{\hat{\sigma}(s)}^i \cdot \mathcal{L}_{match} \left(y_s, \hat{y}_{\hat{\sigma}(s)}^i \right) + \sum_{s=T+1}^N \mathcal{L}_{focal} \left(y_s, \hat{y}_{\hat{\sigma}(s)}^i \right). \quad (12)$$

Finally, the total loss of our MS-DETR is

$$\mathcal{L} = \mathcal{L}^F + \mathcal{L}^V + \mathcal{L}^T. \quad (13)$$

IV. EXPERIMENTS

A. Datasets and Evaluation Metric

Following previous methods, we conduct experiments on three popular datasets, i.e. KAIST, CVC-14 and LLVIP.

KAIST. Originally, the KAIST Multispectral Pedestrian Benchmark [15] contains 95,328 color-thermal image pairs with 103,128 dense annotations covering 1,182 unique pedestrians. For fair comparison with previous methods, we use 7,601 images with sanitized annotations [32] for training and 2,252 images with improved annotations by Liu *et al.* [18] for testing. Specifically, in the test set, 1,455 images are captured during daytime and the remaining during nighttime.

CVC-14. The CVC-14 dataset [30] has 7,085 visible (grayscale) and thermal image pairs for training, where 3,695 pairs are captured during daytime and 3,390 pairs during nighttime. The test set is composed of 1,433 frames. Since the cameras are not well calibrated, the annotations in CVC-14 are individually provided in each modality. Besides, as shown in Fig. 5, the CVC-14 dataset suffers from a severer position shift problem, which makes it more difficult.

LLVIP. LLVIP [31] is a paired visible-infrared dataset for low-light vision. It has 15,488 pairs of aligned images, with 42,437 annotated pedestrians totally. Most of them are taken under the dark scenario by surveillance cameras. The quality of original visible and thermal images in LLVIP dataset is significantly higher than that of the KAIST and CVC-14 datasets. The visible and thermal images have the resolution of 1920×1080 and 1280×720 respectively.

Evaluation metric. For KAIST and CVC-14, we employ the log miss rate (MR^{-2}) averaged over the false positive per image (FPPI) with a range of $[10^{-2}, 10^0]$ for evaluation [15], [51]. A lower MR^{-2} indicates better performance. Moreover, we will report the performance under two evaluation settings for KAIST dataset, i.e. “Reasonable” and “All”. The former only considers the pedestrians taller than 55 pixels with no or partial occlusions while the latter uses whole test data including small or heavy occluded pedestrians. Therefore, the “All” setting is more challenging than “Reasonable” setting.

For LLVIP, we employ the commonly used average precision metrics (AP_{iou}) under different IoU thresholds as evaluation metrics. Specifically, we select $AP_{0.5}$, $AP_{0.75}$, and AP as three metrics for comparison. The AP metric represents the mean AP_{iou} , whose IoU ranging from 0.50 to 0.95 with a stride of 0.05.

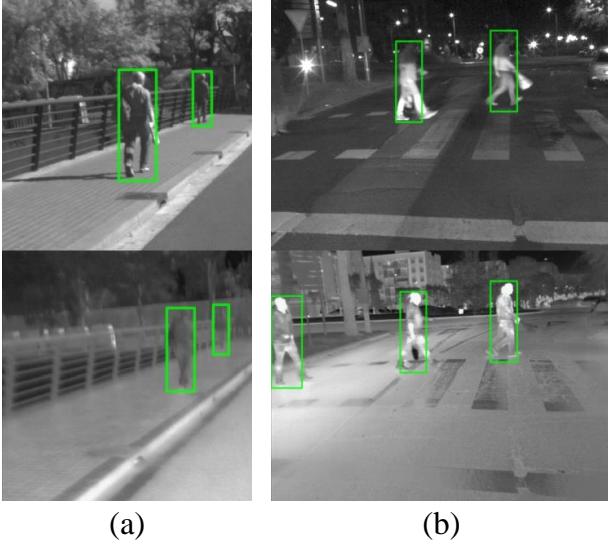


Fig. 5. The visualization examples of position shift problem in CVC-14 dataset, where the pedestrians in (a) are grossly misaligned in spatial dimensions and the number of pedestrians in (b) are unpaired.

B. Implementation Details

Since DETR-like detectors are generally data-hungry [52], we pretrain our model on COCO dataset. In addition to random resize, flip and affine, we also adopt strong data augmentation, including Mixup [53], Mosaic [54] and RandAugment [55].

The proposed MS-DETR is implemented with Pytorch [56]. The backbones for both visible and thermal branches are ResNet50 [57], and the number of feature scales are $L = 4$. Both Transformer encoder and decoder have six layers.

In our multi-modal decoder, the number of attention heads, sampling points, and object queries are set to be $H = 8$, $K = 4$ and $N = 300$. The model is trained using the Adam optimizer [58]. We train it twenty epochs for KAIST and LLVIP datasets, and ten epoches for CVC-14 dataset. The learning rate is initialized as 0.0001 and is decayed at the half of the training process by a factor of ten. The batch size is set to 2.

C. Comparisons with State-of-the-art

KAIST. We compare our model on KAIST dataset with several state-of-the-art methods, including ACF [15], Halfway Fusion [18], Fusion RPN+BF [17], IAF R-CNN [20], IATDNN+IASS [21], CIAN [38], MSDS-RCNN [32], AR-CNN [35], DCRL [23], MBNet [36], CMPD [34], Kim *et al.* [24], MLPD [37] and GAFF [22]. Table I provides the performance comparisons. We can observe our proposed model achieves the best performance under both “Reasonable” and “All” settings, especially under “All” setting, where our MS-DETR outperformed GAFF [22] by 6.66%. Note that the “All” setting is more difficult since it contains small and heavy occluded pedestrians. This performance contrast illustrates that our method can well detect small pedestrians. To validate this, we further evaluate our method on the six subsets in terms of pedestrian distance and occlusion level, whose results are

TABLE III
PERFORMANCE COMPARISONS ON CVC-14 DATASET

Methods	$MR^{-2}(IoU=0.5)$		
	All	Day	Night
MACF [19]	60.1	61.3	48.2
Choi <i>et al.</i> [16]	47.3	49.3	43.8
Halfway Fusion [19]	37.0	38.1	34.4
Park <i>et al.</i> [19]	31.4	31.8	30.8
AR-CNN [35]	22.1	24.7	18.1
MBNet [36]	21.1	24.7	13.5
MLPD [37]	21.3	24.2	18.0
Kim <i>et al.</i> [24]	18.7	23.9	11.1
MS-DETR	16.9	24.1	8.8

shown in Table II. In this table, we can see our method largely reduce the miss rate in almost all cases, except for heavy occluded pedestrians.

Moreover, the FPPI-MR curves on the “Reasonable” and “All” settings are also demonstrated in Fig. 6 and Fig. 7. Under the “Reasonable” setting, our model shows great improvements in the night scenarios, where it obtains the lowest miss rate in a wide range. Furthermore, we can observe from Fig. 7 that MS-DETR has obvious advantages in most FPPI ranges compared to all comparison methods both in daytime and nighttime scenarios. To be specific, our model demonstrates larger superiority than other comparisons at a bigger FPPI under both “Reasonable” and “All” settings.

Finally, we visualize some detection results in Fig. 8, where the yellow rectangles locate the ground truth pedestrians, the green rectangles represent the predictions of MBNet [36], MLPD [37], GAFF [22] and MS-DETR, and red rectangles are missed detection samples of these detectors. From these figures, we can observe that there are some pedestrians missed by the compared methods. In contrast, our model can well locate these challenging samples, especially these small pedestrians. Furthermore, the positive sample confidence scores output by our model is relatively higher than others. We contribute the robust detection of pedestrians to our loosely coupled fusion strategy, which can eliminate the interference of occlusion by fusing the prominent key elements.

CVC-14. Our model is compared with MACF [19], Choi *et al.* [16], Halfway Fusion [18], Park *et al.* [19], AR-CNN [35], MBNet [36], CMPD [34], MLPD [37], and Kim *et al.* [24] on the CVC-14 dataset. Like [36], we fine-tune the model pretrained on the KAIST dataset using the CVC-14. Due to the serious misalignment between visible and thermal modalities in CVC-14 dataset, we also adopt the strategy in [35], where the pedestrians in the visible modality as the training target and the pedestrians in thermal modality as a reference. The final results using dual-modalities are listed in Table III. Note that our model does not have any well-designed alignment modules or operations, but it can also obtain lower miss rate compared with other models, especially in night scenario.

LLVIP. For LLVIP dataset, we compare our method with DCMNet [59], CSAA [60], CFT [61] and LRAF-Net [62]. The results are provided in Table IV. Note that we also present the experimental results of single-modality models. Since LLVIP is a dataset of night scenes, the detection results on thermal modality are generally higher than that on visible modality. In

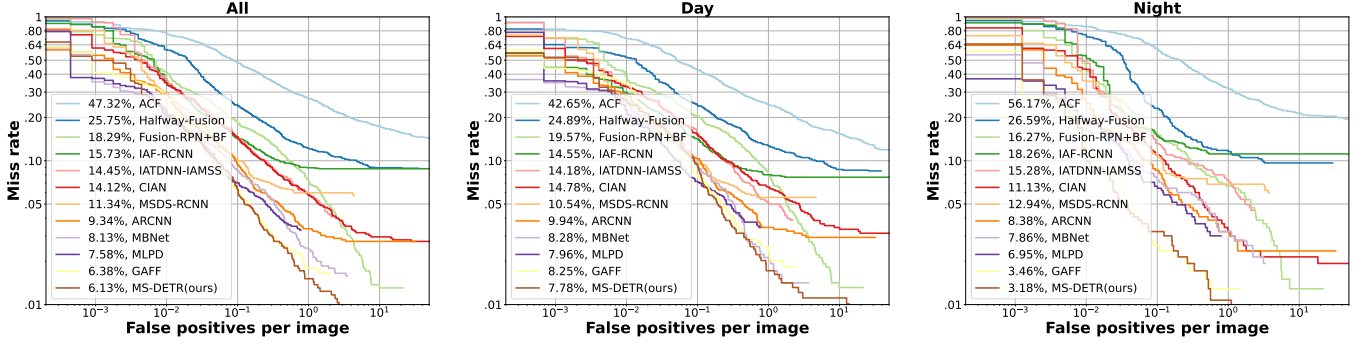


Fig. 6. The FPPI-MR curves comparisons with the state-of-the-art methods on the KAIST dataset under "Reasonable" setting.

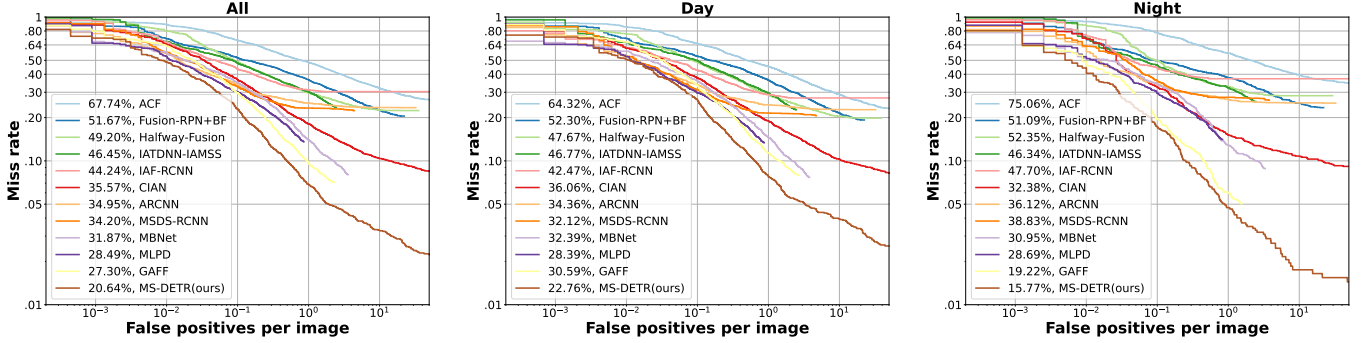


Fig. 7. The FPPI-MR curves comparisons with the state-of-the-art methods on the KAIST dataset under "All" setting.

TABLE IV
COMPARISONS WITH THE STATE-OF-THE-ART METHODS ON THE LLVIP DATASET

Methods	Data	$AP_{0.5}$	$AP_{0.75}$	AP
single-modality				
YOLOv3 [31]	V	85.9	37.9	43.3
YOLOv5 [31]	V	90.8	51.9	50.0
Ours	V	91.8	50.9	50.8
YOLOv3 [31]	T	89.7	53.4	52.8
YOLOv5 [31]	T	94.6	72.2	61.9
Ours	T	97.5	75.1	65.3
multi-modality				
Faster RCNN + DCMNet [59]	V+T	-	-	58.4
Cascade RCNN + DCMNet [59]	V+T	-	-	61.5
RetinaNet + DCMNet [59]	V+T	-	-	58.9
SABL + DCMNet [59]	V+T	-	-	60.6
Reppoints + DCMNet [59]	V+T	-	-	58.7
CSAA [60]	V+T	94.3	66.6	59.2
CFT [61]	V+T	97.5	72.9	63.6
LRAF-Net [62]	V+T	97.9	-	66.3
MS-DETR	V+T	97.9	76.3	66.1

the multi-modality case, our model achieves the comparable performance as LRAF-Net [62] and significantly outperforms other comparison methods. It should be noted that even our single-modality baselines, like the thermal-modality baseline, can obtain superior results than multi-modal comparison methods, which demonstrates the potential of DETR-like models.

D. Ablation Studies

To investigate the effectiveness of our proposed loosely coupled fusion and modality-balanced optimization, we conduct some ablation studies. For simplicity, we only conduct

experiments on KAIST dataset and list the miss rate under both the "Reasonable" and "All" settings.

Effectiveness of loosely coupled fusion strategy. We conduct a series of experiments, including the single-modal detection and the multi-modal detection with different fusion strategies, to verify the effectiveness of proposed loosely coupled fusion. We can firstly observe from Table V that multi-modal detection shows better performance in detecting pedestrians than single-modality by a large margin. Then we investigate the influence of different fusion strategies. In [18], the authors divided the fusion methods into early fusion, halfway fusion and late fusion according to the stage at which the feature fusion operation is performed.

Similarly, our CNN backbone, i.e., ResNet-50, has five stages, named stage-1 to stage-5. Taking the whole Transformer encoder as the last stage, we totally have six stages. Different fusion strategies are defined as follows:

- **Early fusion** begins fusion after stage-1 and shares network parameters from stage-2 to stage-6.
- **Halfway fusion#1** performs fusion from stage-3 to stage-5 and shares networks parameters of stage-6.
- **Halfway fusion#2** is performed after stage-3 and shares from stage-4 to stage-6.
- **Late fusion** only fuses features after stage-6.

As for the fusion process, we first concatenate corresponding features, and then use a 3×3 convolutional layer, followed by batch-normalization and ReLU activation, to obtain the fused features. The results are provided in Table V. When comparing different fusion strategies, we find that late fusion has better performance, and our proposed loosely coupled fusion brings

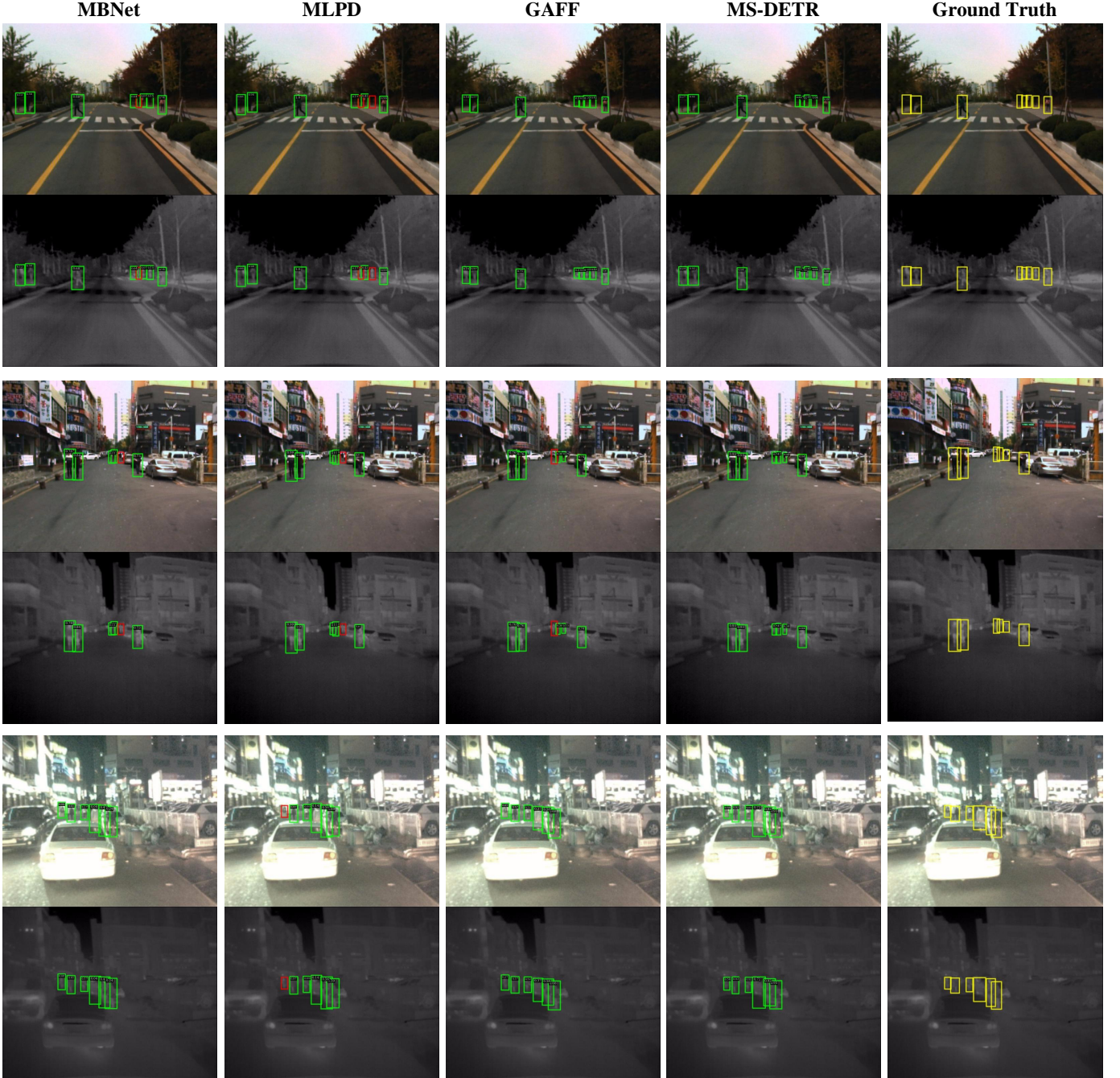


Fig. 8. Some detection results of our model and other three state-of-the-art models on KAIST dataset. The groundtruths, predictions and missed predictions of different detectors are marked in yellow, green and red boxes. Our MS-DETR demonstrates superior results with less miss detections.

the drop of MR^{-2} from 0.15 to 3.49, which validates its effectiveness in DETR-like detection models.

Effectiveness of modality-balanced optimization strategy. To better measure and balance the contribution of visible and thermal modalities, we design an Instance-aware Modality-Balanced Optimization (MBO) strategy, where we select the branch that has minimum cost in current iteration as reference branch to re-arrange the permutation of prediction slots, rather than directly take fusion branch as reference. Further, we employ a dynamic loss to fuse different branches using an instance-level weight. It can be observed from

Table V that the model trained on such a strategy can bring 1.13% drops of MR^{-2} without introducing any additional modules. Therefore, we derive that modality-balanced optimization strategy boosts the detection performance by unifying the permutation of prediction slots and dynamically adjusting the weights of three branches in instance-level.

To investigate its modality balance ability, we present the detection results of all three branches (Fusion, Visible and Thermal) in Table VI. We can find that three branches have balanced detection results under both “All” and “Reasonable” settings, which further proves the effectiveness of MBO strat-

TABLE V
ABLATION STUDIES ON KAIST DATASET. (MBO: Modality-Balanced Optimization)

Modality		Fusion Strategy						Metrics	
Visible	Thermal	Early Fusion	Halfway Fusion#1	Halfway Fusion#2	Late Fusion	Loosely Coupled	MBO	R-All	All
✓								18.18	40.99
	✓							15.61	32.27
✓	✓	✓						10.75	25.46
✓	✓		✓					8.60	24.22
✓	✓			✓				7.96	21.99
✓	✓				✓			7.41	21.58
✓	✓					✓		7.26	21.52
✓	✓					✓	✓	6.13	20.64

TABLE VI
PERFORMANCE COMPARISONS WITHIN THREE DETECTION BRANCH ON KAIST DATASET

Detection Branch	R-All	R-Day	R-Night	All	Day	Night
Visible	6.28	7.98	3.37	20.92	23.19	15.77
Thermal	6.16	7.98	3.22	20.93	23.37	15.94
Fusion	6.13	7.78	3.18	20.64	22.76	15.77

egy.

V. CONCLUSION

This paper presents an end-to-end multispectral pedestrian detector (MS-DETR) via extending the popular DETR framework into the field of multispectral pedestrian detection. A multi-modal Transformer decoder is devised to fuse the visible and thermal features in a loosely coupled fusion way by sparsely sampling some keypoints from the two modalities independently and fusing them with adaptively learned attention weights. Therefore, the loosely coupled fusion strategy can naturally avoid the misalignment issue. In addition, by preserving the visible and thermal branches in the decoder, three sets of predicted slots can be obtained and a novel instance-aware modality-balanced optimization strategy is introduced to measure and adjust the contribution of each instance in visible and thermal images. By a well-designed instance-wise dynamic loss, MS-DETR outperforms existing methods especially on the hard cases, like small or occluded pedestrians.

REFERENCES

- [1] M. Enzweiler and D. M. Gavrila, "Monocular pedestrian detection: Survey and experiments," *IEEE transactions on pattern analysis and machine intelligence*, vol. 31, no. 12, pp. 2179–2195, 2008.
- [2] X. Wang, M. Wang, and W. Li, "Scene-specific pedestrian detection for static video surveillance," *IEEE transactions on pattern analysis and machine intelligence*, vol. 36, no. 2, pp. 361–374, 2013.
- [3] W. Ouyang, X. Zeng, and X. Wang, "Partial occlusion handling in pedestrian detection with a deep model," *IEEE Transactions on Circuits and Systems for Video Technology*, vol. 26, no. 11, pp. 2123–2137, 2015.
- [4] S. Zhang, C. Bauckhage, D. A. Klein, and A. B. Cremers, "Exploring human vision driven features for pedestrian detection," *IEEE Transactions on Circuits and Systems for Video Technology*, vol. 25, no. 10, pp. 1709–1720, 2015.
- [5] Z. Zhang and W. Tao, "Pedestrian detection in binocular stereo sequence based on appearance consistency," *IEEE Transactions on Circuits and Systems for Video Technology*, vol. 26, no. 9, pp. 1772–1785, 2015.
- [6] L. Zhang, L. Lin, X. Liang, and K. He, "Is faster r-cnn doing well for pedestrian detection?" in *European conference on computer vision*. Springer, 2016, pp. 443–457.
- [7] M. Bilal, A. Khan, M. U. K. Khan, and C.-M. Kyung, "A low-complexity pedestrian detection framework for smart video surveillance systems," *IEEE Transactions on Circuits and Systems for Video Technology*, vol. 27, no. 10, pp. 2260–2273, 2016.
- [8] M. Jeong, B. C. Ko, and J.-Y. Nam, "Early detection of sudden pedestrian crossing for safe driving during summer nights," *IEEE transactions on circuits and systems for video technology*, vol. 27, no. 6, pp. 1368–1380, 2016.
- [9] J. Mao, T. Xiao, Y. Jiang, and Z. Cao, "What can help pedestrian detection?" in *Proceedings of the IEEE Conference on Computer Vision and Pattern Recognition*, 2017, pp. 3127–3136.
- [10] C. Lin, J. Lu, and J. Zhou, "Multi-grained deep feature learning for robust pedestrian detection," *IEEE Transactions on Circuits and Systems for Video Technology*, vol. 29, no. 12, pp. 3608–3621, 2018.
- [11] W. Liu, S. Liao, W. Ren, W. Hu, and Y. Yu, "High-level semantic feature detection: A new perspective for pedestrian detection," in *Proceedings of the IEEE/CVF conference on computer vision and pattern recognition*, 2019, pp. 5187–5196.
- [12] Y. Jiao, H. Yao, and C. Xu, "Pen: Pose-embedding network for pedestrian detection," *IEEE Transactions on Circuits and Systems for Video Technology*, vol. 31, no. 3, pp. 1150–1162, 2020.
- [13] K. Kumar and R. K. Mishra, "A diagonally oriented novel feature extractor for pedestrian detection and its efficient hardware implementation," *IEEE Transactions on Circuits and Systems for Video Technology*, vol. 32, no. 4, pp. 2035–2042, 2021.
- [14] C. Li, W. Xia, Y. Yan, B. Luo, and J. Tang, "Segmenting objects in day and night: Edge-conditioned cnn for thermal image semantic segmentation," *IEEE Transactions on Neural Networks and Learning Systems*, vol. 32, no. 7, pp. 3069–3082, 2021.
- [15] S. Hwang, J. Park, N. Kim, Y. Choi, and I. So Kweon, "Multispectral pedestrian detection: Benchmark dataset and baseline," in *Proceedings of the IEEE conference on computer vision and pattern recognition*, 2015, pp. 1037–1045.
- [16] H. Choi, S. Kim, K. Park, and K. Sohn, "Multi-spectral pedestrian detection based on accumulated object proposal with fully convolutional networks," in *2016 23rd International Conference on Pattern Recognition (ICPR)*. IEEE, 2016, pp. 621–626.
- [17] D. Konig, M. Adam, C. Jarvers, G. Layher, H. Neumann, and M. Teutsch, "Fully convolutional region proposal networks for multi-spectral person detection," in *Proceedings of the IEEE Conference on Computer Vision and Pattern Recognition Workshops*, 2017, pp. 49–56.
- [18] J. Liu, S. Zhang, S. Wang, and D. N. Metaxas, "Multispectral deep neural networks for pedestrian detection," in *27th British Machine Vision Conference, BMVC 2016*, 2016.
- [19] K. Park, S. Kim, and K. Sohn, "Unified multi-spectral pedestrian detection based on probabilistic fusion networks," *Pattern Recognition*, vol. 80, pp. 143–155, 2018.
- [20] C. Li, D. Song, R. Tong, and M. Tang, "Illumination-aware faster r-cnn for robust multispectral pedestrian detection," *Pattern Recognition*, vol. 85, pp. 161–171, 2019.
- [21] D. Guan, Y. Cao, J. Yang, Y. Cao, and M. Y. Yang, "Fusion of multispectral data through illumination-aware deep neural networks for pedestrian detection," *Information Fusion*, vol. 50, pp. 148–157, 2019.
- [22] H. Zhang, E. Fromont, S. Lefèvre, and B. Avignon, "Guided attentive feature fusion for multispectral pedestrian detection," in *Proceedings of the IEEE/CVF winter conference on applications of computer vision*, 2021, pp. 72–80.

- [23] T. Liu, K.-M. Lam, R. Zhao, and G. Qiu, "Deep cross-modal representation learning and distillation for illumination-invariant pedestrian detection," *IEEE Transactions on Circuits and Systems for Video Technology*, vol. 32, no. 1, pp. 315–329, 2021.
- [24] J. U. Kim, S. Park, and Y. M. Ro, "Uncertainty-guided cross-modal learning for robust multispectral pedestrian detection," *IEEE Transactions on Circuits and Systems for Video Technology*, vol. 32, no. 3, pp. 1510–1523, 2021.
- [25] S. Ren, K. He, R. Girshick, and J. Sun, "Faster r-cnn: Towards real-time object detection with region proposal networks," *Advances in neural information processing systems*, vol. 28, 2015.
- [26] R. Girshick, J. Donahue, T. Darrell, and J. Malik, "Rich feature hierarchies for accurate object detection and semantic segmentation," in *Proceedings of the IEEE conference on computer vision and pattern recognition*, 2014, pp. 580–587.
- [27] N. Carion, F. Massa, G. Synnaeve, N. Usunier, A. Kirillov, and S. Zagoruyko, "End-to-end object detection with transformers," in *European conference on computer vision*. Springer, 2020, pp. 213–229.
- [28] X. Peng, Y. Wei, A. Deng, D. Wang, and D. Hu, "Balanced multimodal learning via on-the-fly gradient modulation," in *Proceedings of the IEEE/CVF Conference on Computer Vision and Pattern Recognition*, 2022, pp. 8238–8247.
- [29] N. Wu, S. Jastrzebski, K. Cho, and K. J. Geras, "Characterizing and overcoming the greedy nature of learning in multi-modal deep neural networks," in *International Conference on Machine Learning*. PMLR, 2022, pp. 24043–24055.
- [30] A. González, Z. Fang, Y. Socarras, J. Serrat, D. Vázquez, J. Xu, and A. M. López, "Pedestrian detection at day/night time with visible and fir cameras: A comparison," *Sensors*, vol. 16, no. 6, p. 820, 2016.
- [31] X. Jia, C. Zhu, M. Li, W. Tang, and W. Zhou, "Llvp: A visible-infrared paired dataset for low-light vision," in *Proceedings of the IEEE/CVF international conference on computer vision*, 2021, pp. 3496–3504.
- [32] C. Li, D. Song, R. Tong, and M. Tang, "Multispectral pedestrian detection via simultaneous detection and segmentation," in *British Machine Vision Conference (BMVC)*.
- [33] Y. Cao, D. Guan, Y. Wu, J. Yang, Y. Cao, and M. Y. Yang, "Box-level segmentation supervised deep neural networks for accurate and real-time multispectral pedestrian detection," *ISPRS journal of photogrammetry and remote sensing*, vol. 150, pp. 70–79, 2019.
- [34] Q. Li, C. Zhang, Q. Hu, H. Fu, and P. Zhu, "Confidence-aware fusion using Dempster-Shafer theory for multispectral pedestrian detection," *IEEE Transactions on Multimedia*, 2022.
- [35] L. Zhang, X. Zhu, X. Chen, X. Yang, Z. Lei, and Z. Liu, "Weakly aligned cross-modal learning for multispectral pedestrian detection," in *Proceedings of the IEEE/CVF International Conference on Computer Vision*, 2019, pp. 5127–5137.
- [36] K. Zhou, L. Chen, and X. Cao, "Improving multispectral pedestrian detection by addressing modality imbalance problems," in *European Conference on Computer Vision*. Springer, 2020, pp. 787–803.
- [37] J. Kim, H. Kim, T. Kim, N. Kim, and Y. Choi, "Mlpd: Multi-label pedestrian detector in multispectral domain," *IEEE Robotics and Automation Letters*, vol. 6, no. 4, pp. 7846–7853, 2021.
- [38] L. Zhang, Z. Liu, S. Zhang, X. Yang, H. Qiao, K. Huang, and A. Hussain, "Cross-modality interactive attention network for multispectral pedestrian detection," *Information Fusion*, vol. 50, pp. 20–29, 2019.
- [39] H. Zhang, E. Fromont, S. Lefevre, and B. Avignon, "Multispectral fusion for object detection with cyclic fuse-and-refine blocks," in *2020 IEEE International Conference on Image Processing (ICIP)*. IEEE, 2020, pp. 276–280.
- [40] D. Xu, W. Ouyang, E. Ricci, X. Wang, and N. Sebe, "Learning cross-modal deep representations for robust pedestrian detection," in *Proceedings of the IEEE conference on computer vision and pattern recognition*, 2017, pp. 5363–5371.
- [41] H. Zhang, E. Fromont, S. Lefevre, and B. Avignon, "Deep active learning from multispectral data through cross-modality prediction inconsistency," in *2021 IEEE International Conference on Image Processing (ICIP)*. IEEE, 2021, pp. 449–453.
- [42] A. Bulat, R. Guerrero, B. Martinez, and G. Tzimiropoulos, "Fs-detr: Few-shot detection transformer with prompting and without re-training," *arXiv preprint arXiv:2210.04845*, 2022.
- [43] D. Meng, X. Chen, Z. Fan, G. Zeng, H. Li, Y. Yuan, L. Sun, and J. Wang, "Conditional detr for fast training convergence," in *Proceedings of the IEEE/CVF International Conference on Computer Vision*, 2021, pp. 3651–3660.
- [44] Z. Dai, B. Cai, Y. Lin, and J. Chen, "Up-detr: Unsupervised pre-training for object detection with transformers," in *Proceedings of the IEEE/CVF conference on computer vision and pattern recognition*, 2021, pp. 1601–1610.
- [45] X. Dai, Y. Chen, J. Yang, P. Zhang, L. Yuan, and L. Zhang, "Dynamic detr: End-to-end object detection with dynamic attention," in *Proceedings of the IEEE/CVF International Conference on Computer Vision*, 2021, pp. 2988–2997.
- [46] X. Zhu, W. Su, L. Lu, B. Li, X. Wang, and J. Dai, "Deformable detr: Deformable transformers for end-to-end object detection," in *International Conference on Learning Representations*, 2020.
- [47] G. Zhang, Z. Luo, Y. Yu, K. Cui, and S. Lu, "Accelerating detr convergence via semantic-aligned matching," in *Proceedings of the IEEE/CVF Conference on Computer Vision and Pattern Recognition*, 2022, pp. 949–958.
- [48] S. Liu, F. Li, H. Zhang, X. Yang, X. Qi, H. Su, J. Zhu, and L. Zhang, "Dab-detr: Dynamic anchor boxes are better queries for detr," in *International Conference on Learning Representations*, 2021.
- [49] A. Kamath, M. Singh, Y. LeCun, G. Synnaeve, I. Misra, and N. Carion, "Mdetr-modulated detection for end-to-end multi-modal understanding," in *Proceedings of the IEEE/CVF International Conference on Computer Vision*, 2021, pp. 1780–1790.
- [50] M. Maaz, H. Rasheed, S. Khan, F. S. Khan, R. M. Anwer, and M.-H. Yang, "Class-agnostic object detection with multi-modal transformer," in *The European Conference on Computer Vision*. Springer, 2022.
- [51] P. Dollar, C. Wojek, B. Schiele, and P. Perona, "Pedestrian detection: An evaluation of the state of the art," *IEEE transactions on pattern analysis and machine intelligence*, vol. 34, no. 4, pp. 743–761, 2011.
- [52] W. Wang, J. Zhang, Y. Cao, Y. Shen, and D. Tao, "Towards data-efficient detection transformers," in *European conference on computer vision*. Springer, 2022, pp. 88–105.
- [53] H. Zhang, M. Cisse, Y. N. Dauphin, and D. Lopez-Paz, "mixup: Beyond empirical risk minimization," *arXiv preprint arXiv:1710.09412*, 2017.
- [54] A. Bochkovskiy, C.-Y. Wang, and H.-Y. M. Liao, "Yolov4: Optimal speed and accuracy of object detection," *arXiv preprint arXiv:2004.10934*, 2020.
- [55] E. D. Cubuk, B. Zoph, J. Shlens, and Q. V. Le, "RandAugment: Practical automated data augmentation with a reduced search space," in *Proceedings of the IEEE/CVF conference on computer vision and pattern recognition workshops*, 2020, pp. 702–703.
- [56] A. Paszke, S. Gross, F. Massa, A. Lerer, J. Bradbury, G. Chanan, T. Killeen, Z. Lin, N. Gimelshein, L. Antiga et al., "Pytorch: An imperative style, high-performance deep learning library," *Advances in neural information processing systems*, vol. 32, 2019.
- [57] K. He, X. Zhang, S. Ren, and J. Sun, "Deep residual learning for image recognition," in *Proceedings of the IEEE conference on computer vision and pattern recognition*, 2016, pp. 770–778.
- [58] I. Loshchilov and F. Hutter, "Decoupled weight decay regularization," *arXiv preprint arXiv:1711.05101*, 2017.
- [59] J. Xie, R. M. Anwer, H. Cholakkal, J. Nie, J. Cao, J. Laaksonen, and F. S. Khan, "Learning a dynamic cross-modal network for multispectral pedestrian detection," in *Proceedings of the 30th ACM International Conference on Multimedia*, 2022, pp. 4043–4052.
- [60] Y. Cao, J. Bin, J. Hamari, E. Blasch, and Z. Liu, "Multimodal object detection by channel switching and spatial attention," in *Proceedings of the IEEE/CVF Conference on Computer Vision and Pattern Recognition*, 2023, pp. 403–411.
- [61] F. Qingyun, H. Dapeng, and W. Zhaokui, "Cross-modality fusion transformer for multispectral object detection," *arXiv preprint arXiv:2111.00273*, 2021.
- [62] H. Fu, S. Wang, P. Duan, C. Xiao, R. Dian, S. Li, and Z. Li, "Lraf-net: Long-range attention fusion network for visible-infrared object detection," *IEEE Transactions on Neural Networks and Learning Systems*, 2023.